27
9-21-76
25 to NTIS

UCID- 17184

Lawrence Livermore Laboratory

A STUDY OF CORE CHIPS FROM THE STATE OF CALIFORNIA WELL NO. 1 IN THE SALTON SEA GEOTHERMAL FIELD USING PETROGRAPHIC, X-RAY DIFFRACTION, AND SCANNING ELECTRON MICROSCOPY TECHNIQUES

L. Dengler
A. J. Piwinskii

August 13, 1976

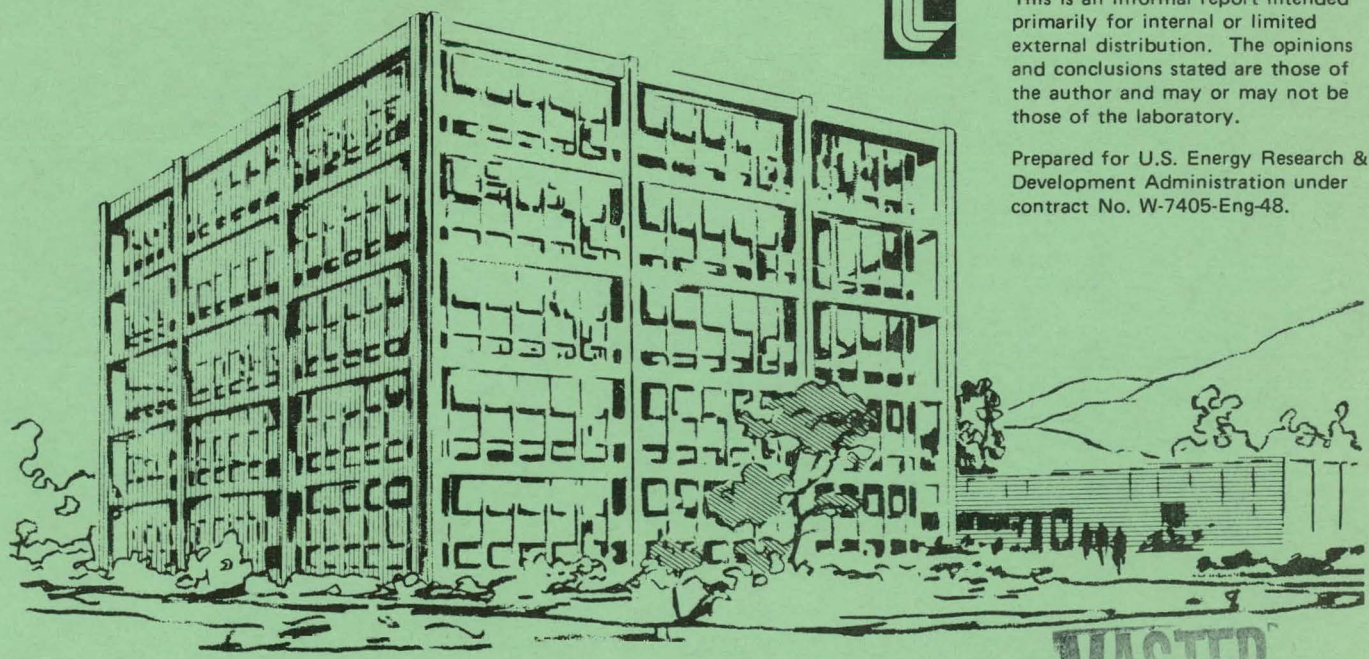

Prepared for U.S. Energy Research & Development Administration under contract No. W-7405-Eng-48.

DISCLAIMER

A STUDY OF CORE CHIPS FROM THE STATE OF CALIFORNIA WELL NO. 1 IN THE SALTON SEA GEOTHERMAL FIELD USING PETROGRAPHIC, X-RAY DIFFRACTION, AND SCANNING ELECTRON MICROSCOPY TECHNIQUES

ABSTRACT

Rock chips from depths of 1380 to 1478 m from the State of California Well No. 1 in the Salton Sea Geothermal Field were examined using conventional petrographic, x-ray diffraction, and scanning electron microscopy techniques. Mineral composition, pore configuration and the nature of the fine-grained matrix materials were determined.

INTRODUCTION

To characterize porous media of the Salton Sea Geothermal Field prior to reinjection studies, we examined core chips of sedimentary rocks from the State of California Well No. 1 obtained from the depth interval of 1379.7 to 1478.0 m (see Figs. 1 and 2). The samples studied are listed in Table 1.

Table 1. Samples examined from various depths from State of California Well No. 1.

Material	Sample number	Depth (m)
Dense grey siltstone	SS1	1379.7
Grey-massive siltstone	SS7	1399.1
Green-grey siltstone	SS2	1400.0
Dark grey siltstone	SS3	1476.2
Grey silty sandstone	SS4	1477.7
Brown-grey sandstone	SS5	1477.8
Light grey sandstone	SS6	1478.0

The temperature distribution of the State of California Well No. 1 as a function of depth is presented in Fig. 3 (See Ref. 1) and the composition of the saline brine from this well is reported in Table 2. It is evident that the samples investigated were simultaneously exposed to the highest temperatures recorded in the well (approximately 300°C) and highly saline fluids.

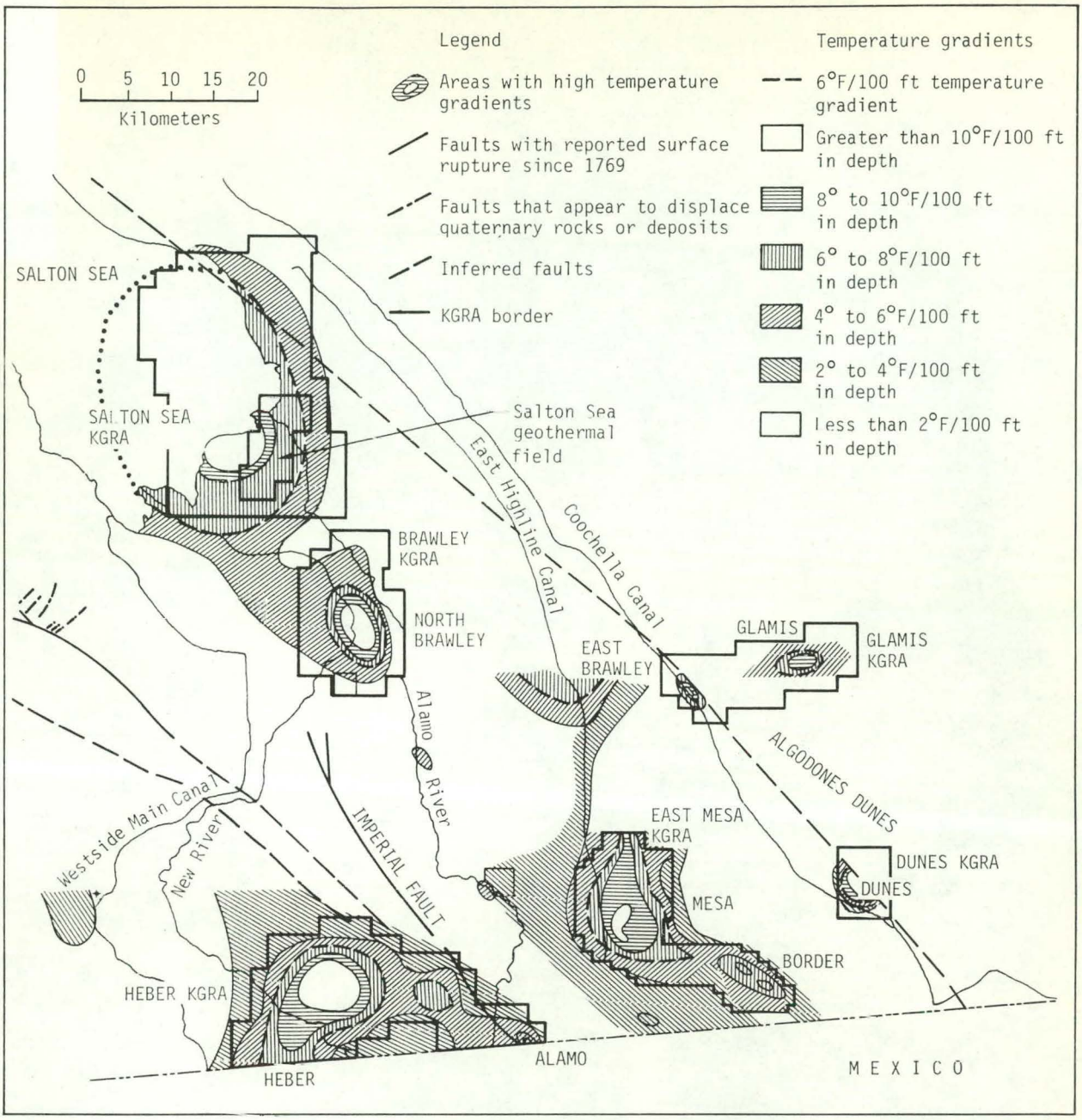

Fig. 1. Temperature gradient map of the Imperial Valley, California showing the Known Geothermal Resource Areas (KGRA) and the Salton Sea Geothermal Field. Temperature gradient compiled and interpreted by J. Combs, University of California, Riverside, Sept. 1971.

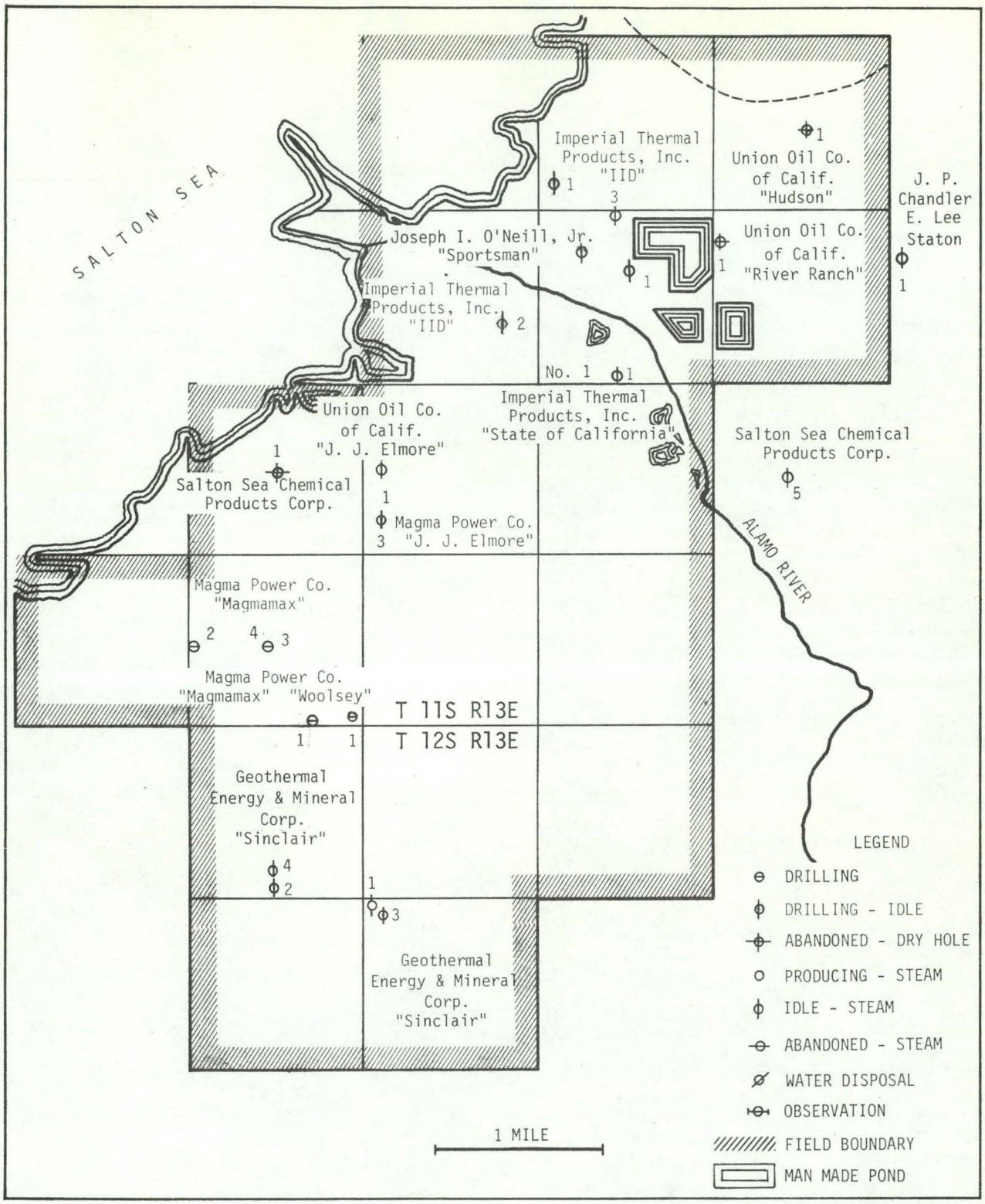

Fig. 2. Location of geothermal wells in the Salton Sea Geothermal Field. Base from U.S.G.S. topographic map: well information supplied by California Division of Oil and Gas.

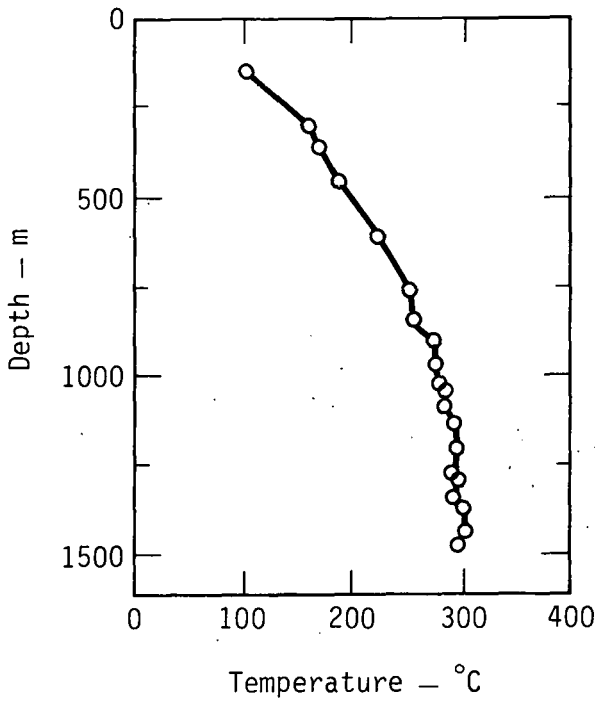

Fig. 3. Temperature vs depth for the State of California Well No. 1.[1]

Table 2. Composition in ppm by Weight of Brine from State of California Well No. 1.[a]

Constituent	Amount
Sodium	47,800
Potassium	14,000
Lithium	180
Barium	190
Calcium	21,200
Strontium	not listed
Magnesium	27
Boron	290
Silica	not listed
Iron	1,200
Manganese	950
Lead	80
Zinc	500
Copper	2
Silver	<1
Rubidium	65
Cesium	17
Chloride	127,000
Σ CO_2	5,000
Σ S	30
Total Dissolved Solids	219,500

[a]Analysis from H. C. Helgeson, "Geologic and Thermodynamic Characteristics of the Salton Sea Geothermal System," Amer. Sci. 266, 129 (1968).

SCOPE OF THE INVESTIGATION

This study was concentrated in three areas: x-ray diffraction analysis (XRD), optical microscopy, and scanning electron microscopy (SEM). Powder diffraction of bulk rock chips was used for XRD analysis. For optical microscopy, conventional thin section analysis was employed to determine minerology, petrography, and grain size distribution. Two thin sections of each rock specimen were examined, one perpendicular and the other parallel to the bedding. For SEM analysis, tensional fracture faces of one or two specimens

of each rock were investigated to obtain an approximate analysis of the pore configuration, and the nature of fine-grained matrix materials. (See Dengler[2] for a detailed description of the method of specimen preparation for SEM analysis.)

RESULTS

Dense Grey Siltstone: SS1

This specimen has well-developed graded bedding as shown in Fig. 4. Its principal mineral constituents are quartz and K-feldspar with minor quantities of calcite, plagioclase, and chlorite.[3] This specimen possesses the lowest total clay content of all the rocks studied. The presence of authigenic K-feldspar, quartz (both phases as large as 50 μm in diameter), hematite, magnetite, and slight amounts of pyrite was revealed by petrographic examination of thin sections of SS1 (see Fig. 5).

A SEM photomicrograph of this sample is shown in Fig. 6. Matrix grain diameters range from 2 to 16 μm with a mean of 10 μm. Clay minerals average 1 μm long by 0.1 μm wide. An enlargement of region A is seen in Fig. 6b; region A is composed of euhedral cubic crystals, possibly magnetite.

The pore structure of SS1 is visible in Fig. 6c, an enlargement of region B in Fig. 6. The pore structure is not well-defined and the maximum pore diameters observed in SS1 are approximately 2 μm.

Grey-Massive Siltstone: SS7

The rock possesses highly contorted bedding and appears distinctly green in thin section (Fig. 7). The major minerals are quartz and chlorite. SS7 contains approximately 30% clay minerals, the highest percentage clay in this series of samples. Moderate amounts of illite/K-mica,[4] K-feldspar, and plagioclase are present. SS7 possesses the lowest amount of feldspar of the rocks studied. Calcite was not detected in bulk rock XRD. Some pyrite and epidote (Fig. 8) were also detected in thin section.

An SEM photomicrograph of SS7 is shown in Fig. 9a. This low magnification view illustrates the heterogeneity of this specimen. Figure 9b shows the contact between the two beds at a much higher magnification and reveals that these two areas are composed of distinctly different mineral phases. Figures 10a and b, enlargements of the left and right beds respectively, substantiate this. The material in Fig. 10a is almost entirely clay, probably chlorite, while the stubby two-phase assemblage in Fig. 10b is quartz and feldspar.

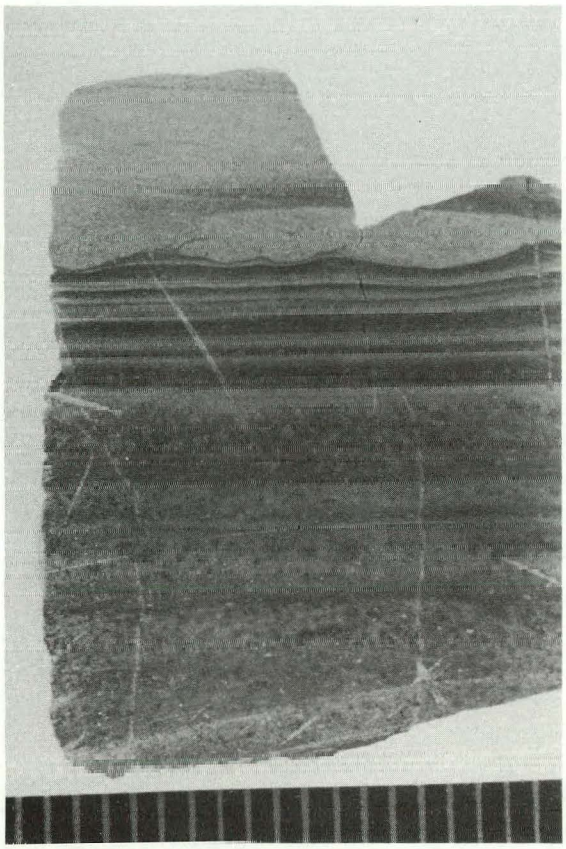

Fig. 4. Siltstone SS1 showing the well-developed graded bedding and fine grain size (scale in millimeters).

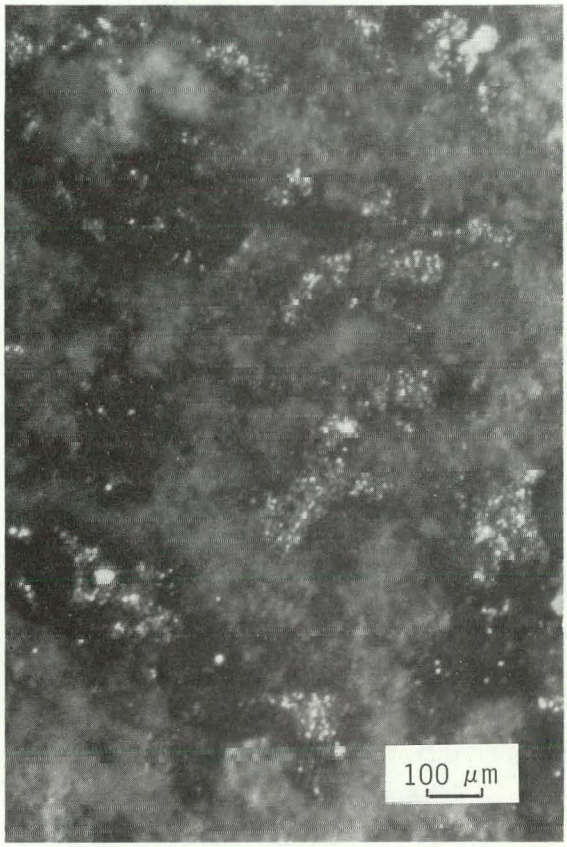

Fig. 5. Optical photomicrograph of siltstone SS1 in reflected light: dark areas are hematite and lighter speckled areas are pyrite.

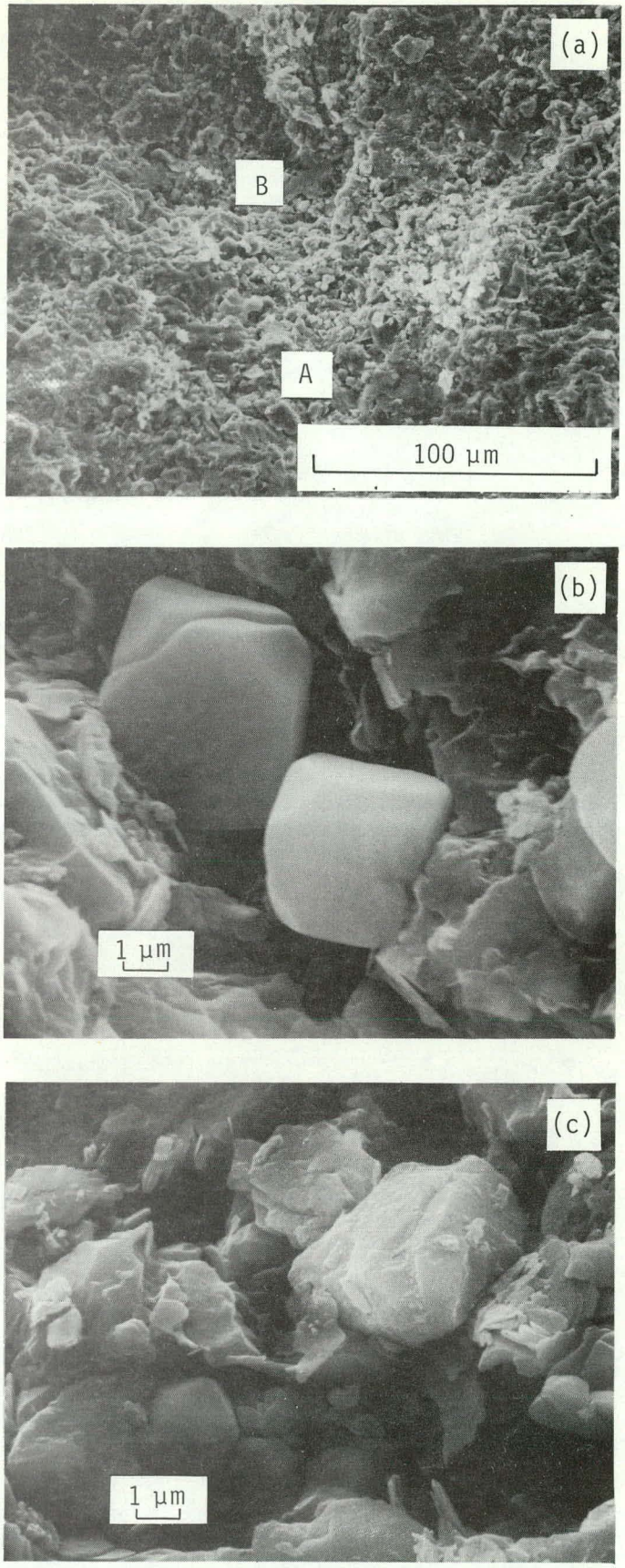

Fig. 6. SEM photomicrograph of SS1 (a) and enlargements of regions A (b) and B (c). In (b), the cubic crystals are possibly magnetite. The typical pore configuration of SS1 is shown in (c).

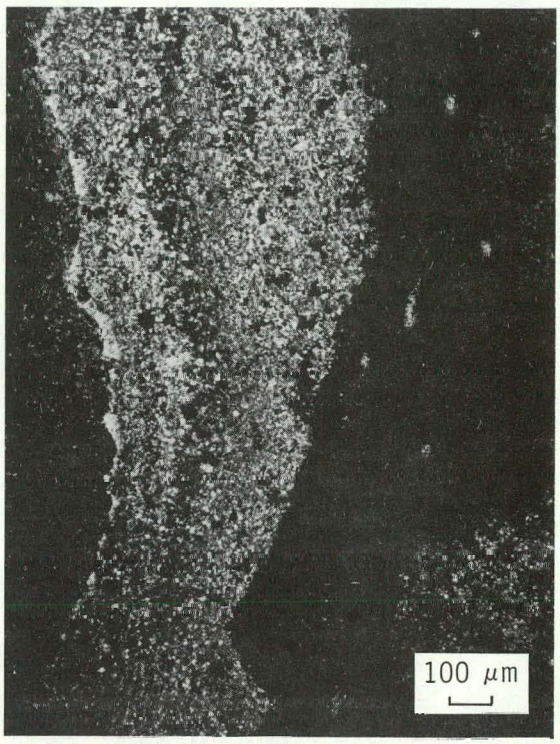

Fig. 7. Optical photomicrograph of SS7 in doubly polarized light: dark areas are mainly chlorite.

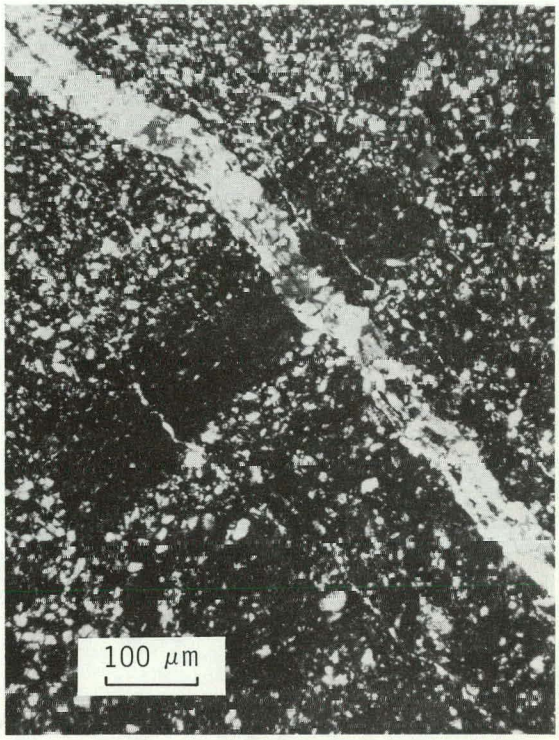

Fig. 8. Optical photomicrograph of SS7 in doubly polarized light showing an epidote vein.

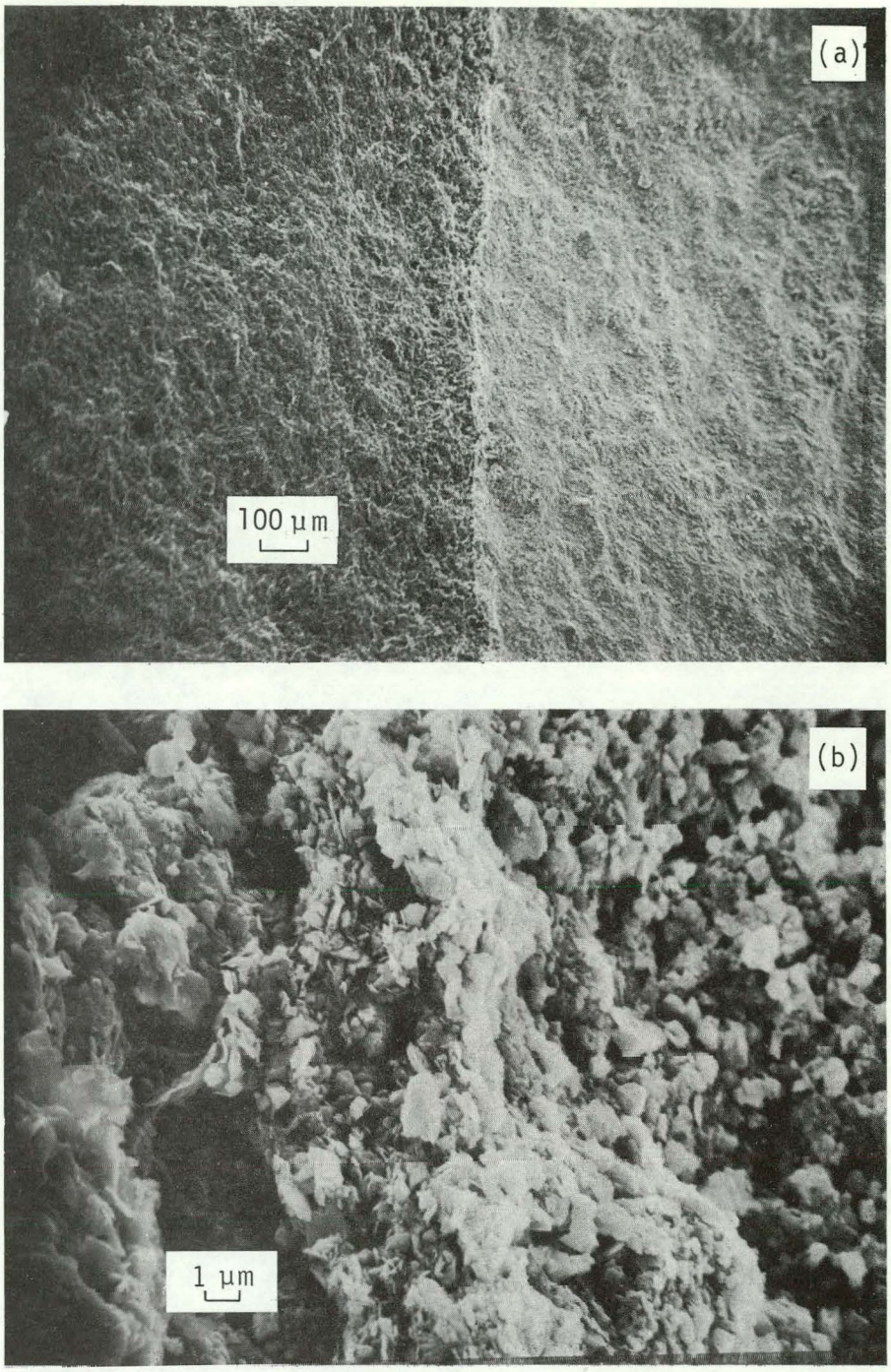

Fig. 9. SEM photomicrograph of SS7 bedding structure (a), and an enlargement of the contact area between the two beds (b).

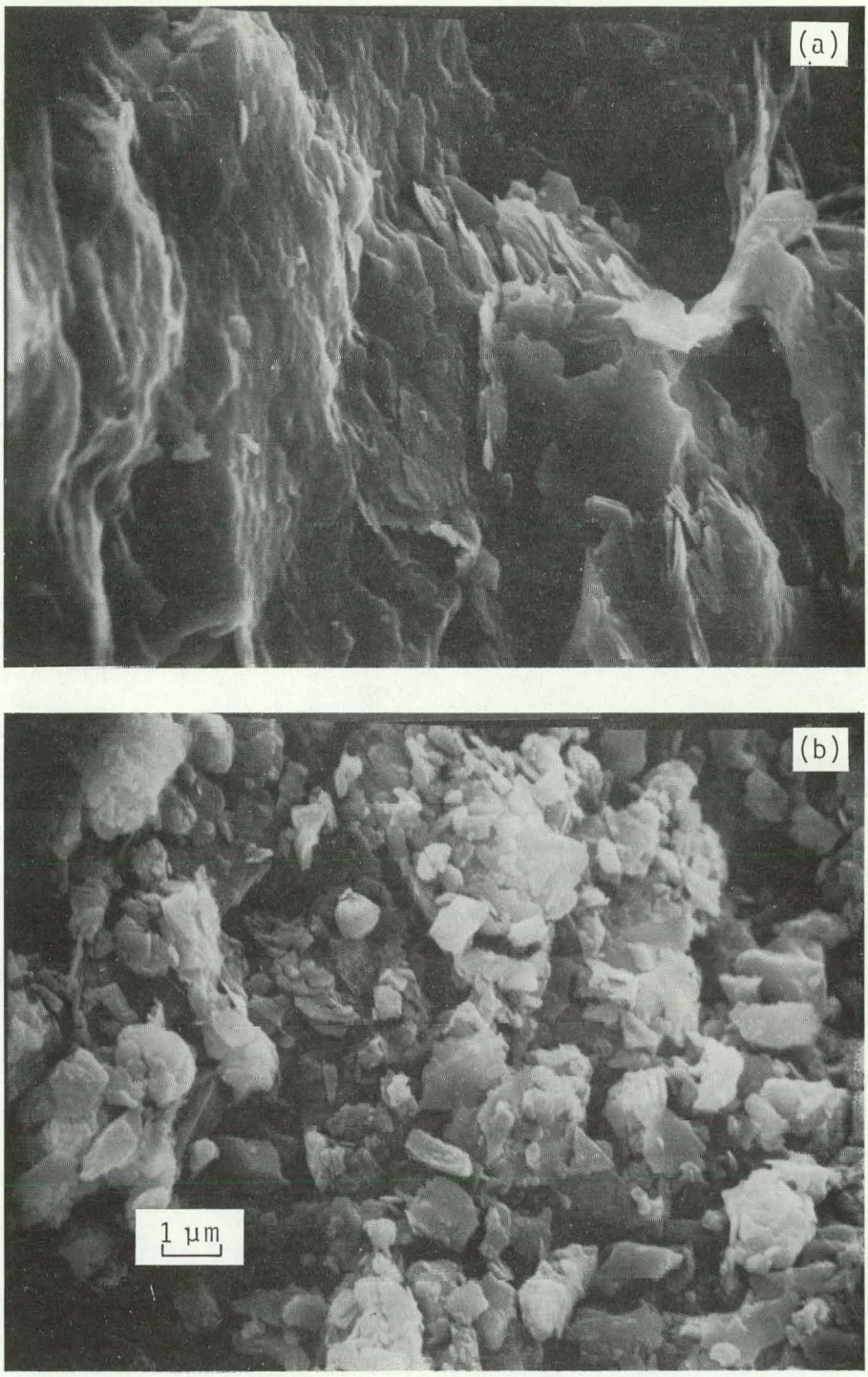

Fig. 10. SEM photomicrograph of left (a) and right (b) beds shown in Fig. 9. The bed in (a) is composed entirely of clay (probably chlorite) whereas the bed in (b) is composed of quartz and feldspar grains.

The mineral stratification illustrated in Fig. 10 has a profound influence on the nature of the pore structure in SS7. Porosity in the clay beds is extremely low because there is virtually no visible pore space. The quartz-feldspar regions appear to be more porous with pore diameters of approximately 1 μm.

Green-Grey Silstone: SS2

This sample is characterized by well-developed graded bedding and lenses of detrital quartz and K-feldspar (up to 40 μm in diameter). These two features are displayed in Fig. 11, an optical photomicrograph of SS2. The principal minerals are quartz and K-feldspar with moderate amounts of plagioclase and chlorite. Calcite and illite/K-mica were not detected in bulk rock x-ray diffraction analyses. Pyrite was observed in thin section but, because of its presence in small quantities, it was undetected in x-ray analyses of the bulk rock. When observed under partially reflected light, euhedral pyrite grains up to 300 μm in diameter can be seen (Fig. 12).

The SEM photomicrograph of SS2 (Fig. 13a), illustrates the general rock fabric and mineral habit. Quartz grains in the matrix average 20 μm in diameter and tend to be enveloped by clay minerals. This is seen clearly in Fig. 13b, a higher magnification detail of Fig. 13a. The pore and clay structures can be seen in Fig. 13c, an enlarged view of region A in Fig. 13b. Pore diameters correspond to submicron size cracks between clay plates, suggesting that the porosity of SS2 is very low.

Dark Grey Silstone: SS3

This specimen displays bedding and is composed principally of quartz, K-feldspar, and calcite. Minor amounts of plagioclase, chlorite, and illite/K-mica are also present. Of all the chips studied, SS3 possesses the highest illite/K-mica content. Small amounts of pyrite were identified in thin section. An optical photomicrograph of SS3 is presented in Fig. 14 where, because of their opacity in transmitted light, pyrite grains are seen as black regions.

Fossil foraminifera fragments in varying stages of replacement by pyrite (see lower-central region of Fig. 14) were an interesting discovery in this sample. An SEM photomicrograph of SS3 showing clay minerals enveloping the foraminifera is shown in Fig. 15a. Crystals of pyrite have replaced both foraminifera in the center of the picture. In Fig. 15b, an enlargement of the right-central foraminifer, pyrite octahedra and pyritohedra can be seen growing in an interconnected honeycomb pattern.

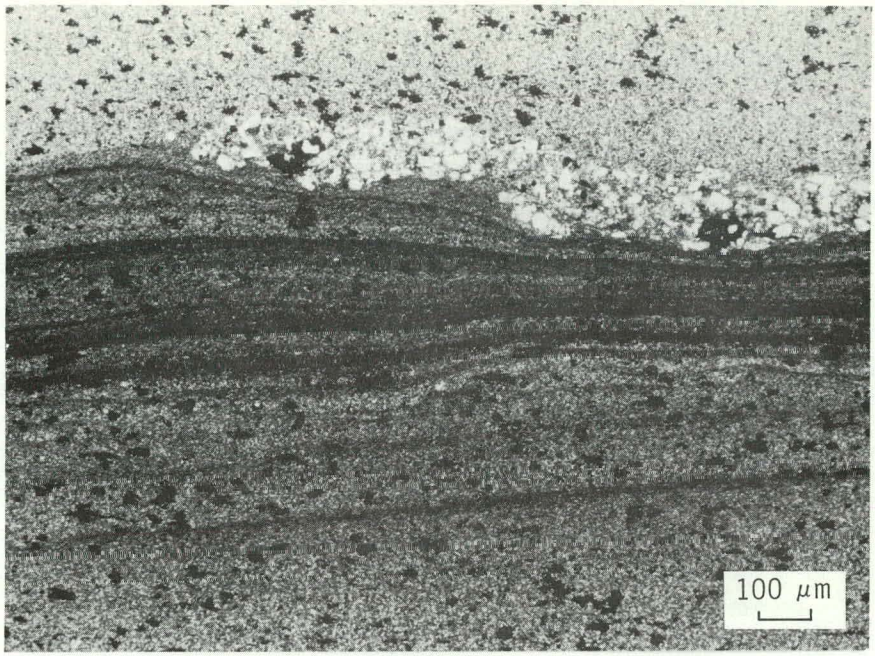

Fig. 11. Optical photomicrograph of SS2 showing the graded bedding and lenses of coarser detrital quartz and feldspar.

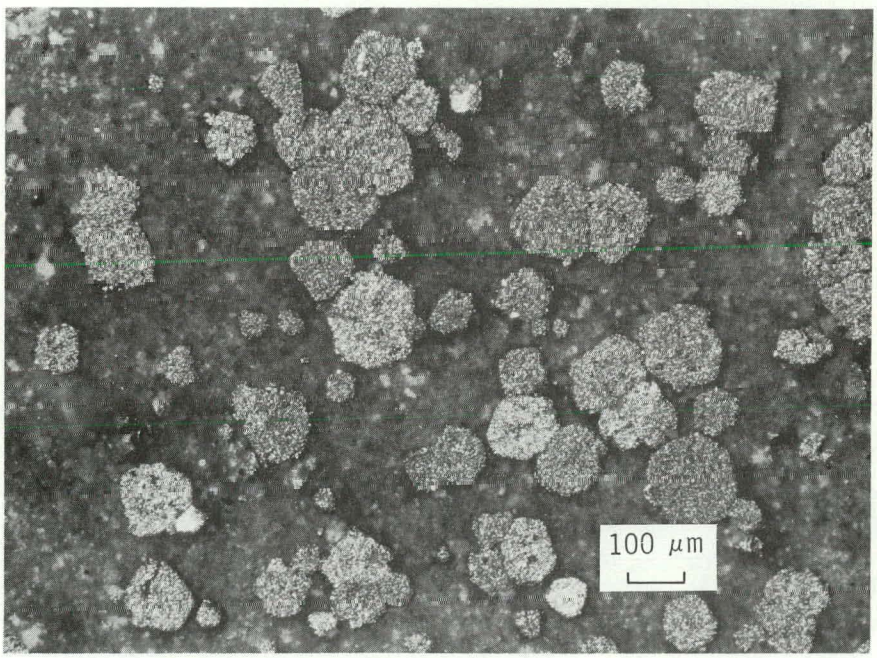

Fig. 12. Optical photomicrograph of SS2 in partially reflected light. Subhedral and euhedral grains are pyrite: hackled surfaces of the sulfides are an artifact of grinding during thin section preparation.

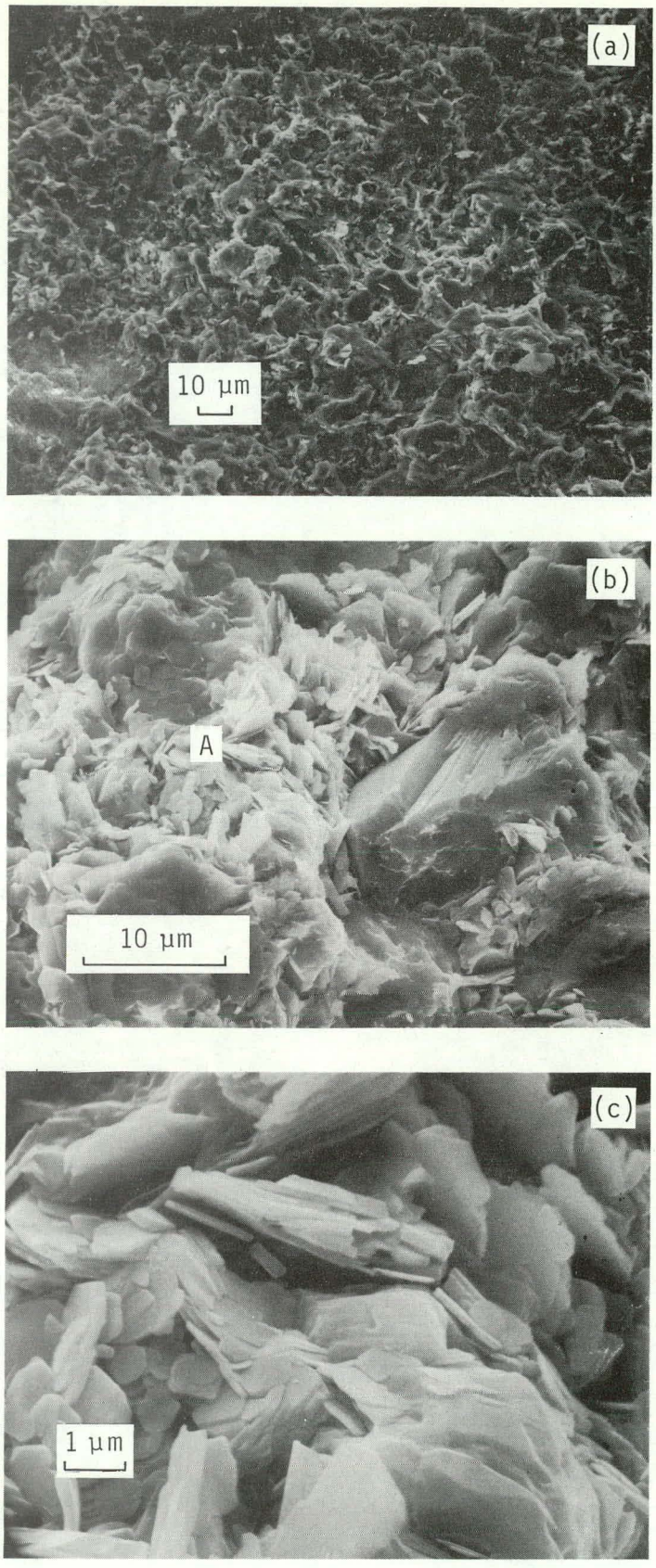

Fig. 13. SEM photomicrograph of SS2 (a) and enlargements (b and c). The stubby euhedral quartz and feldspar grains surrounded by flaky clay minerals can be seen in (b). The details of clay and pore structure are shown in (c), an enlargement of region A in (b).

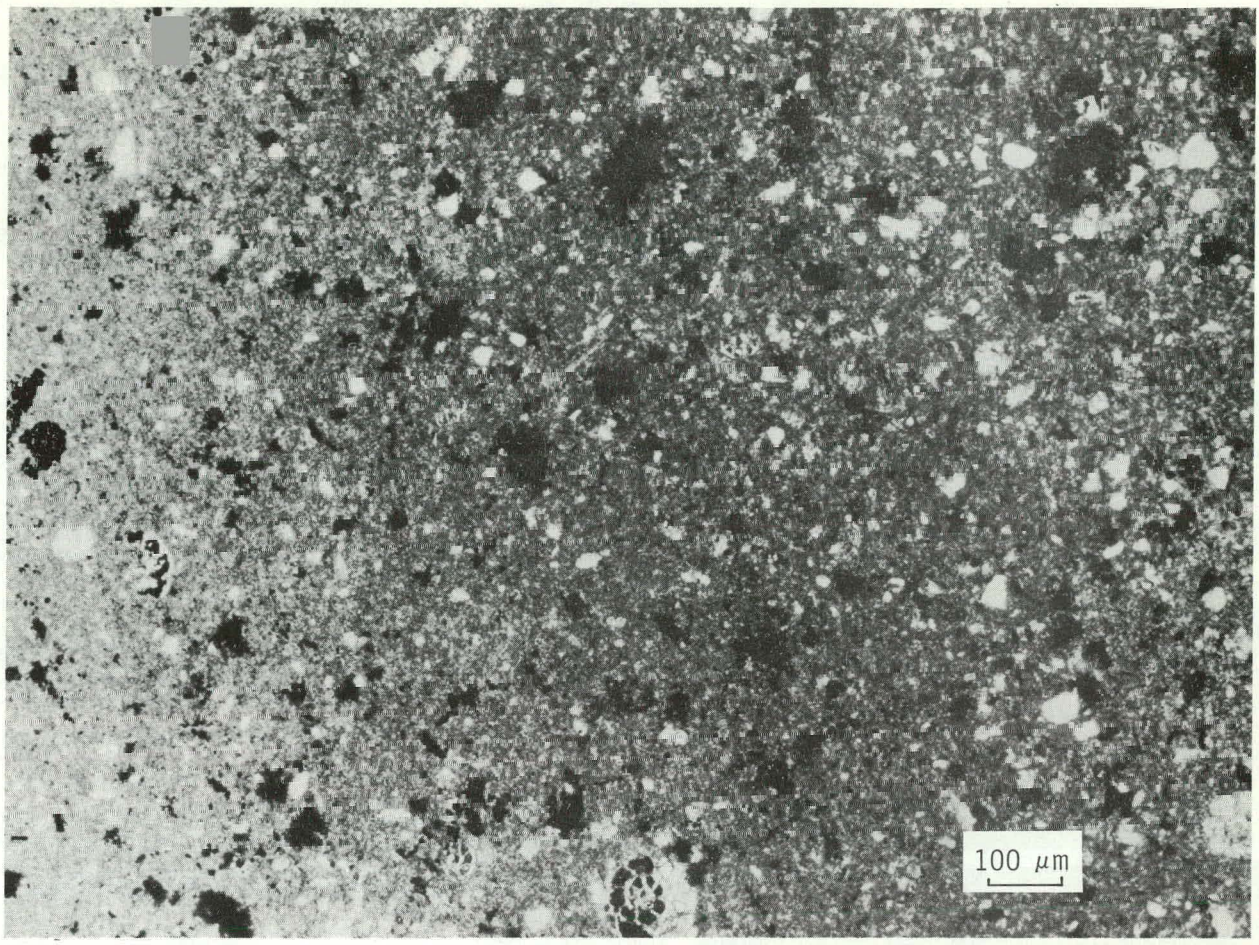

Fig. 14. Optical photomicrograph of siltstone SS3. Fossil fragments of foraminifera are dispersed in a quartz-feldspar matrix: black regions in the fossils are pyrite.

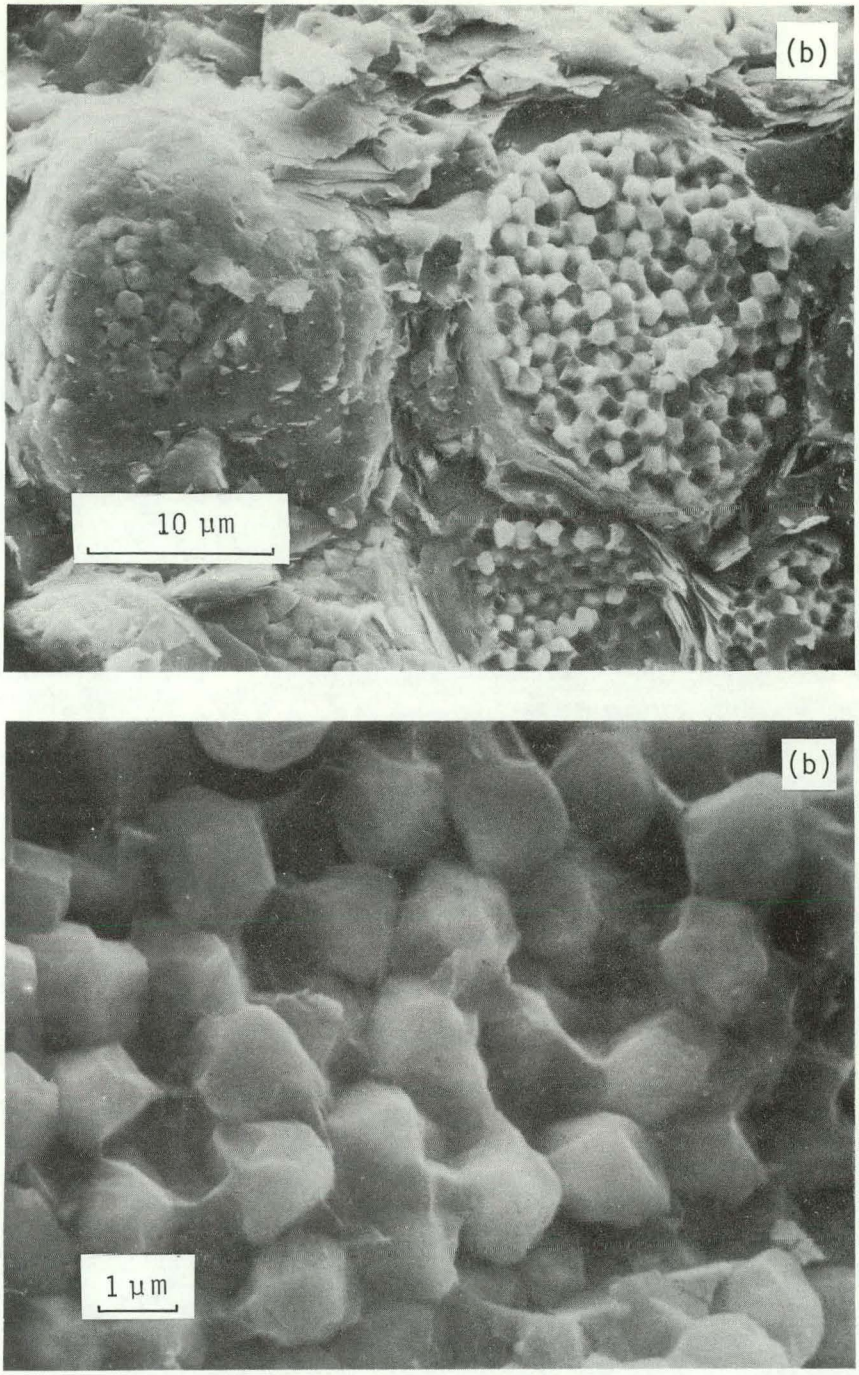

Fig. 15. SEM photomicrograph of SS3 showing clay minerals enveloping the foraminifera that are being replaced by pyrite (a). An enlargement of the right-central foraminifer (b) shows pyrite octahedra and pyritohedra growing in an interconnected honeycomb pattern, replacing the original foraminifer test.

Matrix grain diameters average 5 μm with the clay minerals exhibiting much finer dimensions. The pore structures seen in region above the foraminifera in Fig. 15a are also very small with maximum pore diameters of approximately 1 μm.

Grey Silty Sandstone: SS4

This sedimentary rock is characterized by poorly developed bedding. The major minerals are quartz, calcite, and K-feldspar; plagioclase and chlorite are present in minor amounts. No illite/K-mica was detected in the x-ray diffraction patterns. Thin section studies indicated that the concentration of quartz is highly variable, even over the area of the thin section. Occasional grains of pyrite were also seen in thin section.

An SEM photomicrograph of SS4 is given in Fig. 16a and an enlarged view of region A is seen in Fig. 16b. Quartz grain diameters vary from 10 to 50 μm and maximum pore diameters are approximately 1 μm.

Brown-Grey Sandstone: SS5

Bedding is not pronounced in this sample. The principal mineral constituents are quartz, K-feldspar, and calcite with moderate amounts of plagioclase, chlorite, and illite/K-mica. Thin section examination also revealed the presence of some pyrite.

An SEM study of SS5 showed that the sample is extremely variable in both mineralogy and pore structure over the SEM sample size (approximately 10 mm in diameter). Large grains of quartz with diameters up to 100 μm were frequently observed in a finer matrix (particle size of approximately 20 μm). In Fig. 17a, the large detrital quartz fragment can be seen surrounded by a matrix of authigenic quartz, feldspar, and clay minerals.

Locally heavy concentrations of clays up to 50 μm in area were noted during the SEM study of SS5. Figure 17b illustrates one regional high population possessing a habit similar to kaolinite. Some populations are characterized by different orientations of clay plates that give rise to very different pore configurations. This is seen in Fig. 17c, an enlargement of Fig. 17b. The virtual absence of porosity in this region is evident. Because of the heterogeneity of SS5, pore sizes vary from less than 0.1 μm up to 2 to 3 μm.

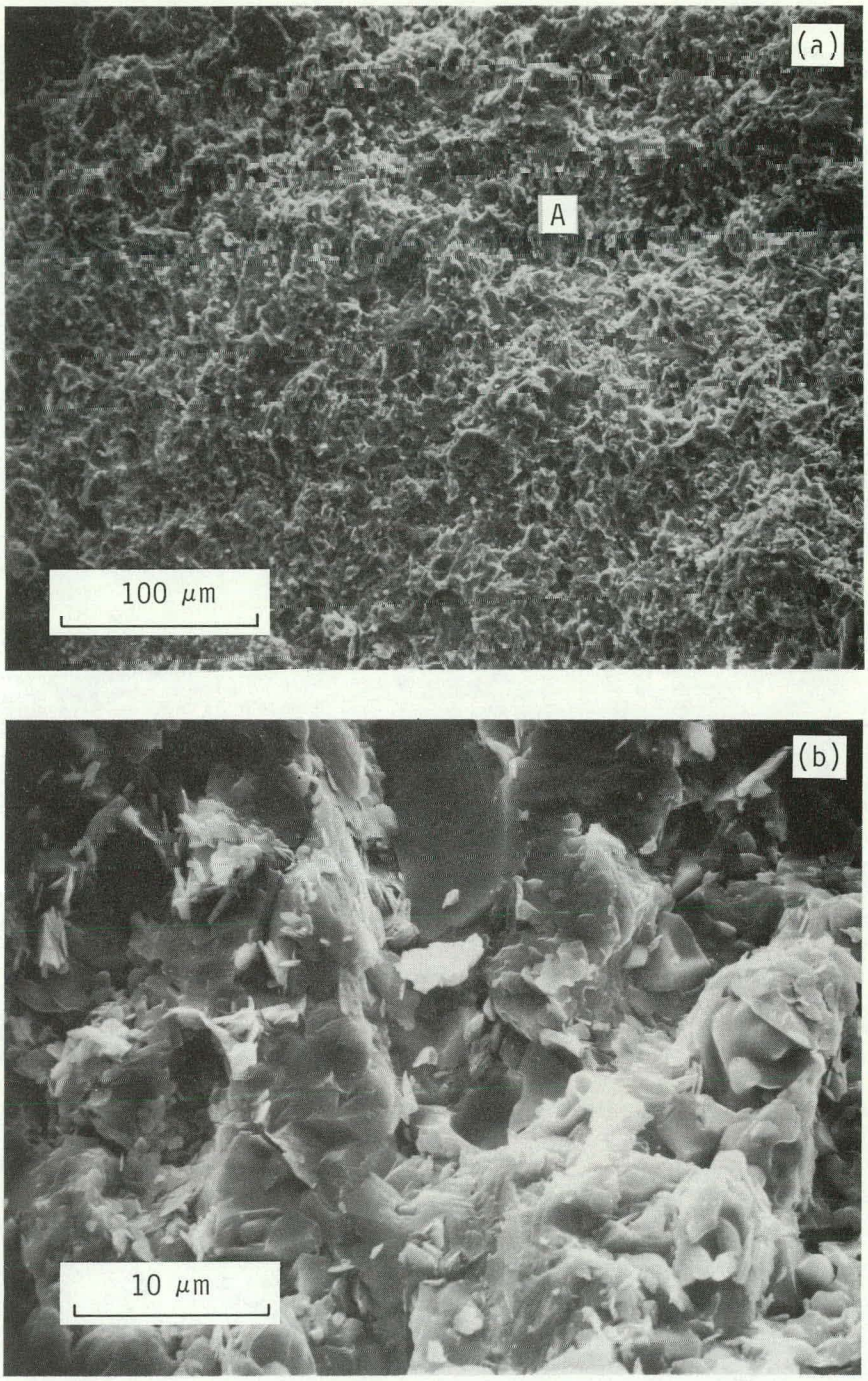

Fig. 16. SEM photomicrograph of sandstone SS4 (a) and an enlargement of region A (b) showing pore structure.

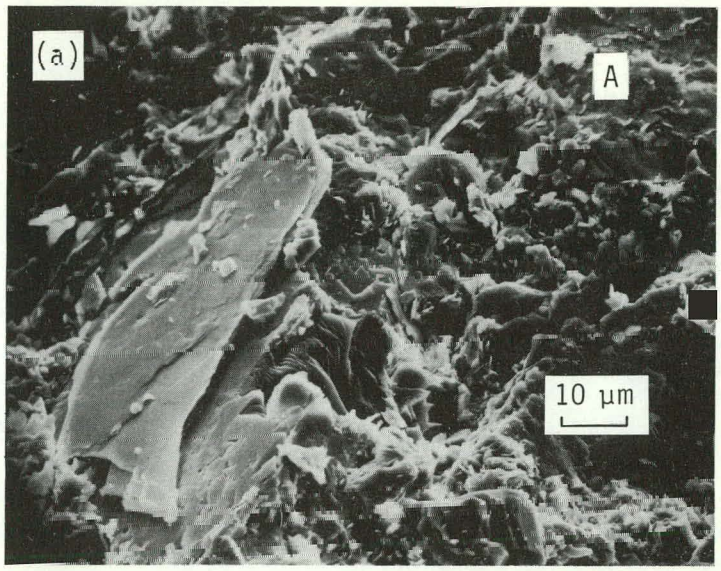

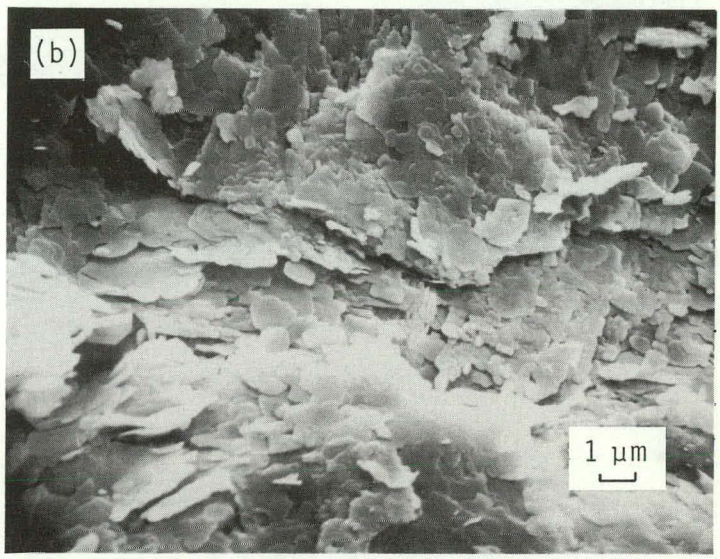

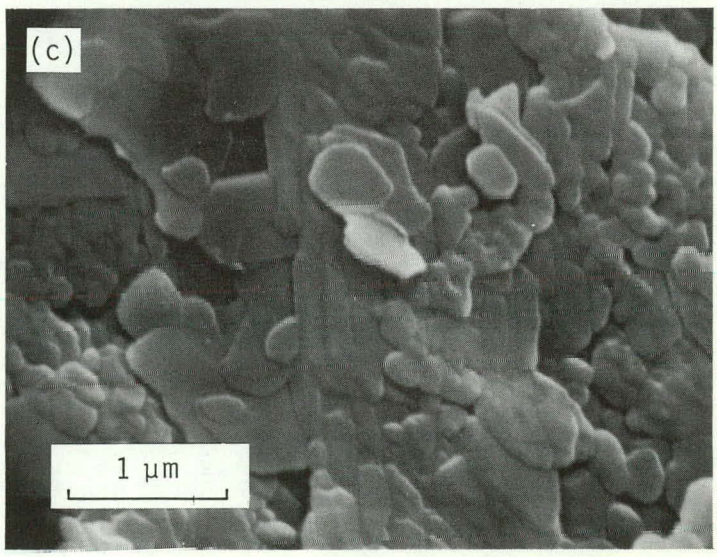

Fig. 17. SEM photomicrograph of sandstone SS5 (a) and enlargements of region A (b and c). In (a), a detrital quartz grain is surrounded by a matrix of authigenic quartz, feldspar, and clays. A large clay population with habit similar to kaolinite is shown in (b). In (c), an enlargement of (b), the finely detailed clay structure and virtual absence of porosity can be seen.

Light Grey Sandstone: SS6

This sample possesses poorly-developed bedding. Its major constituent minerals are quartz, calcite, plagioclase, and K-feldspar. It possesses the highest calcite content of all the samples studied (Fig. 18). Moderate amounts of chlorite are present and traces of pyrite were identified in thin section.

SS6 is highly variable in grain size as shown by the SEM study. Figure 19a depicts a detrital feldspar grain set in a finer grained matrix ranging from 2 to 80 μm in particle size. Authigenic quartz and feldspar enclosed in finer clay matrix are seen in Fig. 19b. An enlargement of the previous figure illustrating details of the clay structure is shown in Fig. 19c. Mineral alteration is observed optically and with SEM. Figure 20a illustrates the possible alteration of a detrital feldspar fragment. Finer details of the alteration products are clearly observed in Fig. 20b. SS6 is highly variable in pore structure with typical pore dimensions of 2 to 3 μm.

SUMMARY AND CONCLUSIONS

Rock chips in the depth interval of 1380 to 1478 m from State of California Well No. 1 were examined using conventional petrographic, x-ray diffraction and SEM methods. These specimens were found to be dense, well-indurated siltstones with occasional sand-size detrital grains. Authigenic feldspar and quartz were observed in all samples, indicative of late-stage, post-depositional precipitation and alteration. Presence of small amounts of pyrite in all samples and as a replacement mineral in original foraminifera tests (see Figs. 14 and 15) indicates a protracted exposure to infiltrating hypersaline brine in the temperature interval of 200 to 300°C. Presence of co-existing authigenic quartz and iron sulphides suggests a reducing environment at pH greater than 3.5 at a temperature of 200°C for a brine of Sinclair No. 4 composition.[5]

Results of the x-ray diffraction[6] analyses (see Fig. 21) are generally consistent with Muffler and White's results[6] on the IID No. 1 and Sportsman No. 1 wells , also located in the Salton Sea Geothermal Field. Data on the SS7 sample indicate low values of K-feldspar and high quantities of chlorite relative to the other samples from this depth range. However, because only one x-ray diffraction scan was performed on each chip, some of these variations in relative mineral composition may be merely a result of sample heterogeneities.

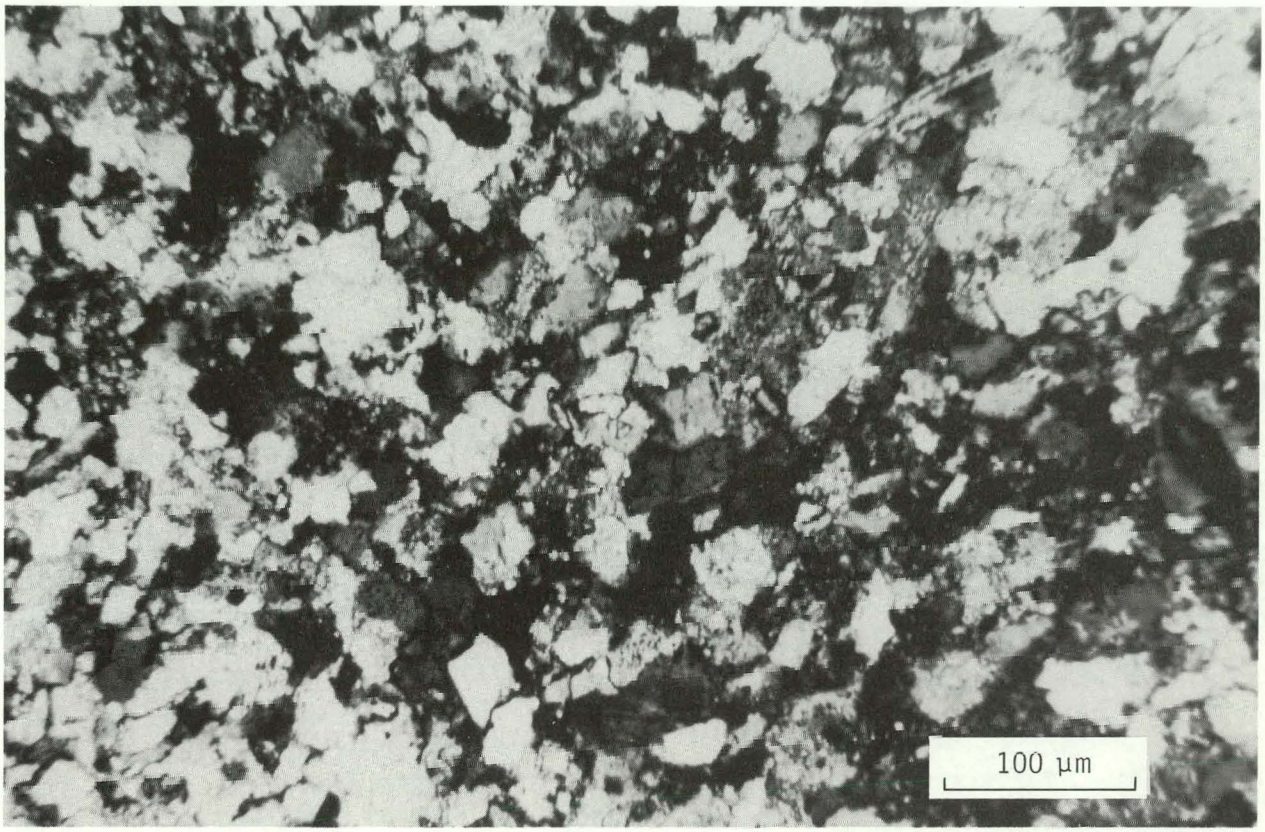

Fig. 18. Optical photomicrograph of SS6 in doubly polarized light.

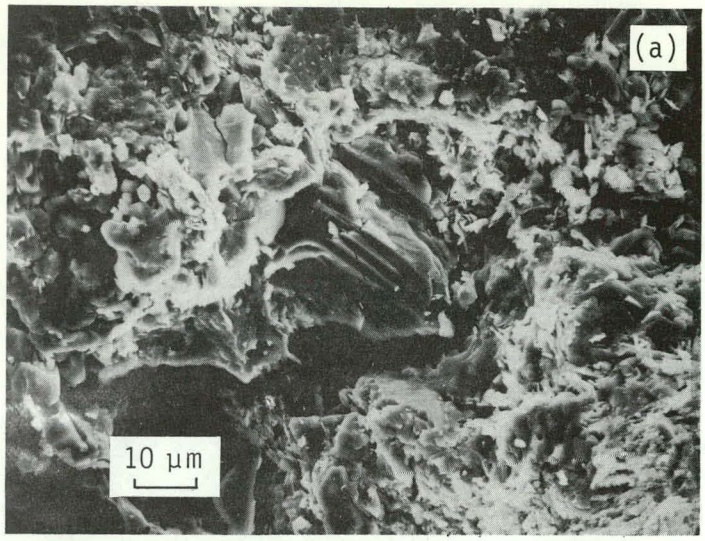

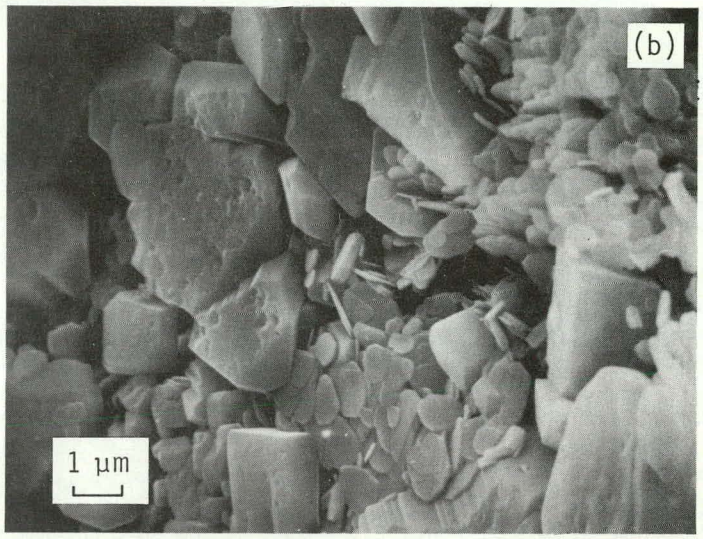

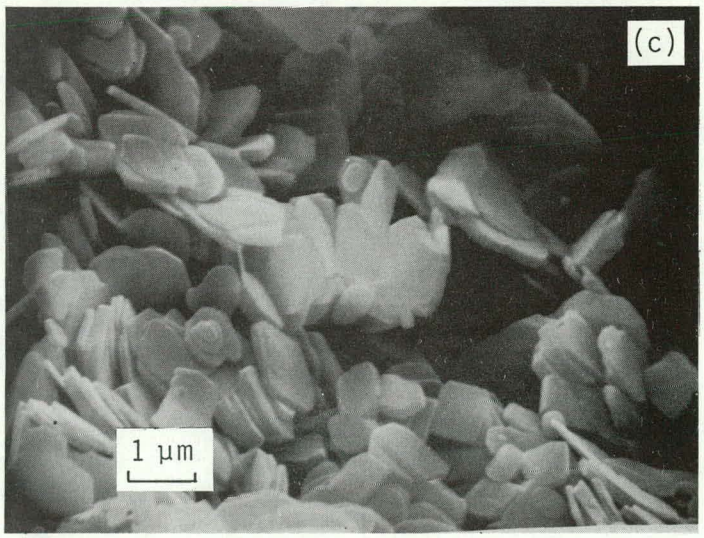

Fig. 19. SEM photomicrograph of sandstone SS6 (a) and enlargements (b and c). In (a), a detrital feldspar grain is set in a finer grained matrix: the diagonal crack probably occurred during sample preparation. The stubby euhedral quartz and feldspar grains surrounded by clays are shown in (b). In (c), an enlargement of (b), the thin layer structure of the clays and a pore (right center) can be seen.

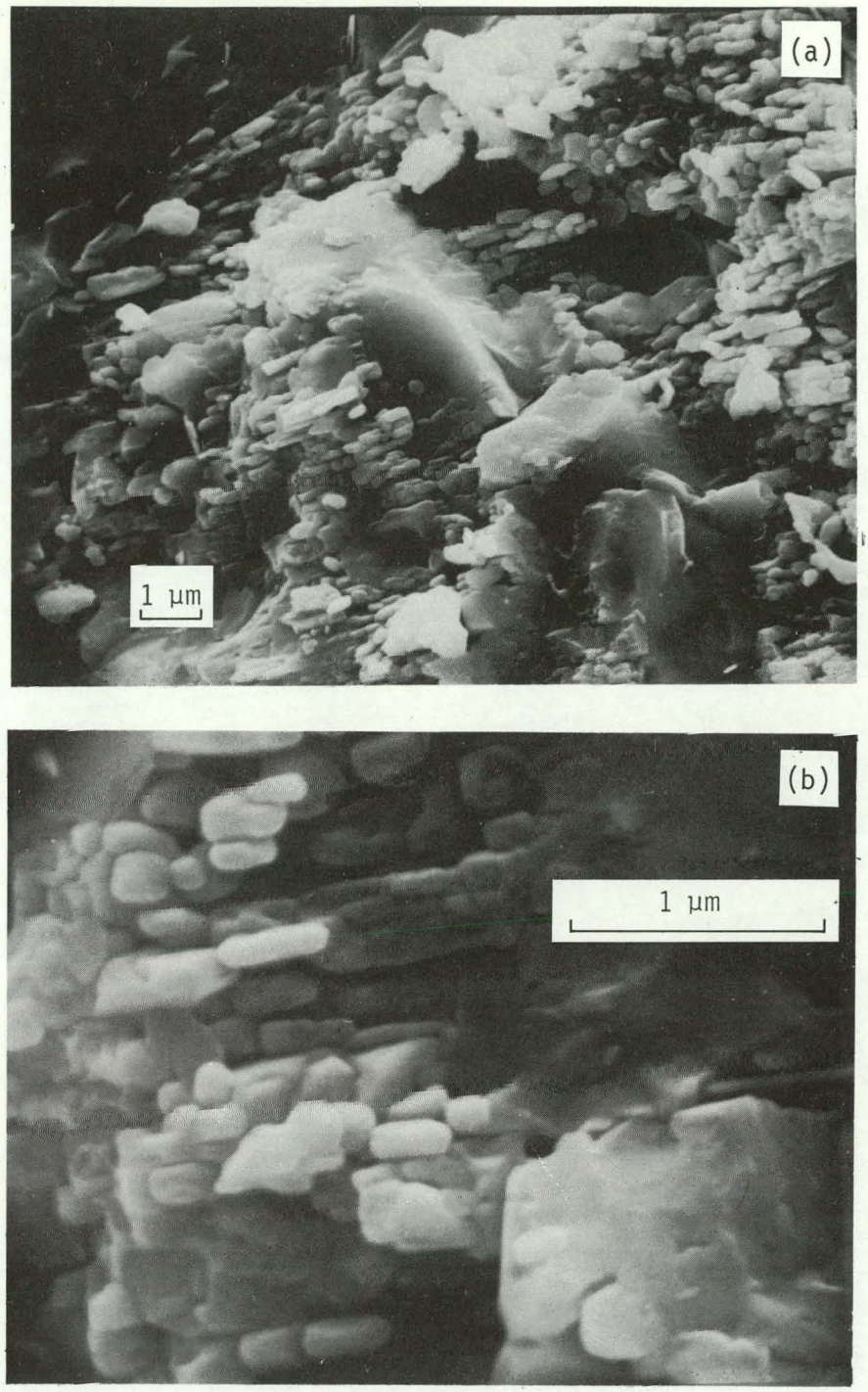

Fig. 20. SEM photomicrograph of SS6 illustrating the possible alteration of a detrital feldspar fragment (a) and an enlargement (b) showing finer details of the alteration products.

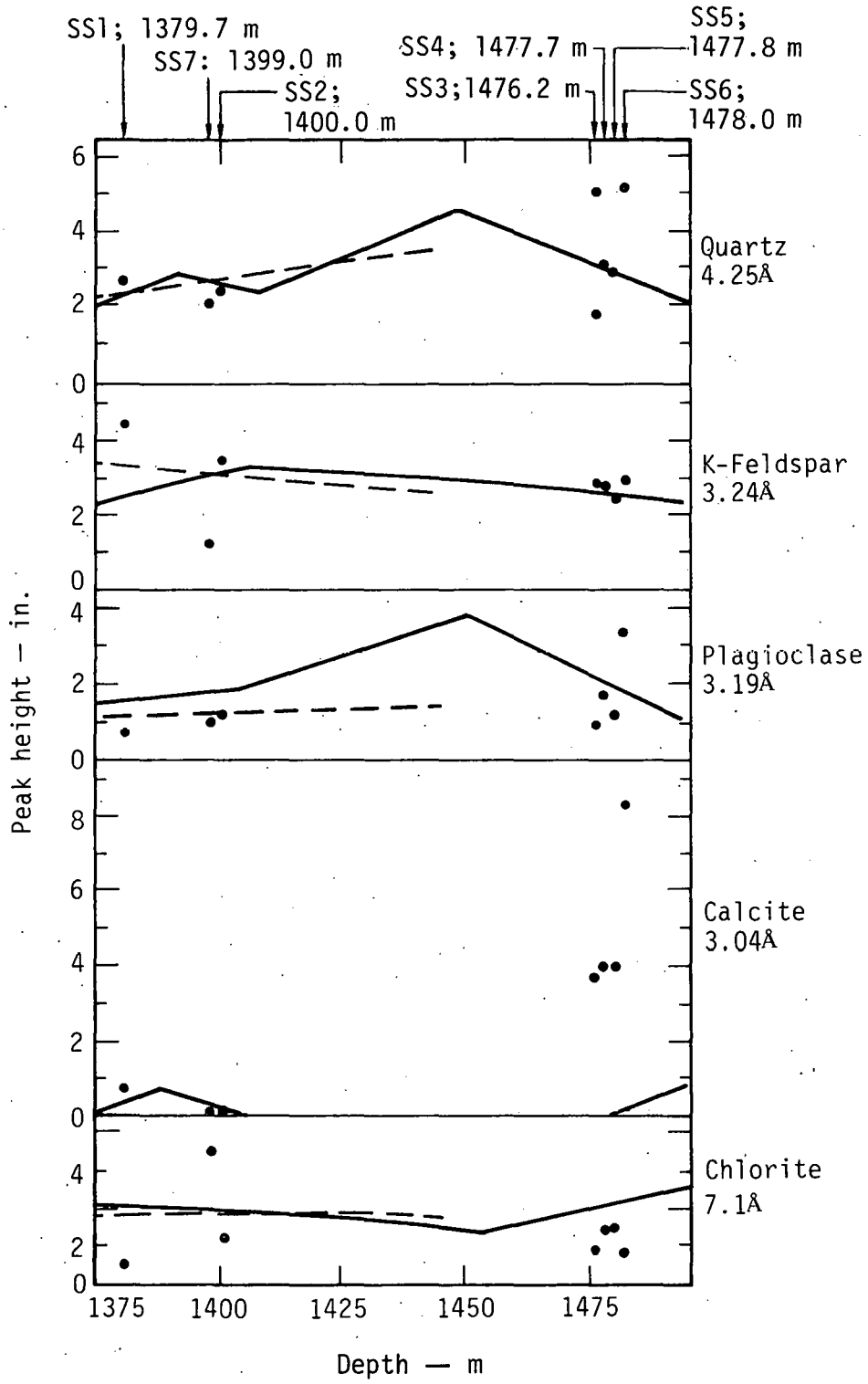

Fig. 21. Occurrence of minerals as a function of depth for State of California No. 1 (•), IID No. 1 (solid line), and Sportsman No. 1 wells (dashed line).[5]

It is interesting that the 1400-m horizon (samples SS7 and SS2) is devoid of calcite. Muffler and White's analysis of IID No. 1 samples also revealed no calcite at that depth. These results suggest that a regional calcite-free horizon may exist in the 1400- to 1450-m depth interval.

NOTES AND REFERENCES

1. T. Palmer, *Characteristics of Geothermal Wells Located in the Salton Sea Geothermal Field, Imperial County, California*, Lawrence Livermore Laboratory, Rept. UCRL-51976 (1975).
2. L. A. Dengler, *The Effect of Stress on the Microstructure of a Graywacke Sandstone from the Site of Rio Blanco Gas Stimulation Experiment*, Lawrence Livermore Laboratory, Rept. UCRL-51919 (1975).
3. It is very difficult, if not impossible in some cases, to differentiate kaolinite from chlorite by XRD analysis because the high intensity (001) basal reflection of kaolinite is 7.16 Å,[7] while the high intensity (002) reflection for monoclinic chlorites ranges between 7.02 to 7.18 Å.[8] We distinguished chlorite from kaolinite by first heating the sample to 500°C, and then reanalyzing it. The XRD analysis still revealed the presence of the 7.1 Å peak, thus indicating that the clay fraction is chlorite and not kaolinite. We also verified that a 14 Å peak in the pattern was a secondary chlorite peak and not montmorillinite (15 Å) by glycolating the specimen overnight. The results of this test were negative for montmorillinite. Thus, because glycol will enter a "montmorillinite-type mineral and cause a characteristic expansion of the basal spacing to about 17.5 Å",[8] we attribute the 14 Å peak to chlorite.
4. Throughout this paper, we report the 10 Å peak as illite/K-mica. The high intensity (002) reflection of illite ranges between 9.98 to 10.1 Å, while the same reflection in mica lies between 9.99 and 10.1 Å.[9] Illite was originally defined[10] as a general term for mica-like clay minerals with the formula

$$K_y (Si_{8-y} \cdot Al_y) (Al_4 \cdot Fe_4 \cdot Mg_4 \cdot Mg_6) O_{20}(OH)_4$$

where y equals 2.0 for mica and y is less than 2.0 for illite. One effective method to differentiate illite from K-mica is by the location of secondary peaks in the 1.4- to 1.6-Å range. However for our samples, the (002) reflection at approximately 10 Å was very weak when detected at all. Therefore, it was not possible to detect the weaker secondary reflections in bulk XRD analyses of rock chips.

5. D. Jackson, A. J. Piwinskii, and D. Miller, "Computational Methods for Estimating Precipitation from Geothermal Brines," abstract in *Symposium on Scale Management and Geothermal Energy Development, 1976* (University of California, San Diego, 1976), p. 1.

6. L. J. Muffler and D. White, "Active Metamorphosism of Upper Cenozoic Sediments in the Salton Sea Geothermal Field and Salton Trough, Southeastern California," *Geol. Soc. Amer. Bull.* 80, 157 (1969).

7. G. Brindley and K. Robinson, "Randomness in the Structures of Kaolinitic Clay Minerals," *Trans. Faraday Soc.* 42B, 198 (1946).

8. G. Brindley, "Chlorite Minerals," in *The X-Ray Identification and Crystal Structures of Clay Minerals*, G. Brown, Ed. (Mineralogical Society of London, London, 1961), pp. 242-296.

9. W. Bradley and R. Grim, "Mica Clay Minerals," in *The X-Ray Identification and Crystal Structures of Clay Minerals*, G. Brown, Ed. (Mineralogical Society of London, London, 1961), pp. 208-241.

10. R. Grim, R. Bray, and W. Bradley, "The Mica in Argillaceous Sediments," *Amer. Mineral.* 22, 813 (1937).

Printed in the United States of America
Available from
National Technical Information Service
U.S. Department of Commerce
5285 Port Royal Road
Springfield, VA 22161
Price: Printed Copy $; Microfiche $2.25

Page Range	Domestic Price	Page Range	Domestic Price
001–025	$ 3.50	326–350	10.00
026–050	4.00	351–375	10.50
051–075	4.50	376–400	10.75
076–100	5.00	401–425	11.00
101–125	5.25	426–450	11.75
126–150	5.50	451–475	12.00
151–175	6.00	476–500	12.50
176–200	7.50	501–525	12.75
201–225	7.75	526–550	13.00
226–250	8.00	551–575	13.50
251–275	9.00	576–600	13.75
276–300	9.25	601–up	*
301–325	9.75		

*Add $2.50 for each additional 100 page increment from 601 to 1,000 pages: add $4.50 for each additional 100 page increment over 1,000 pages.

PLL/np/vt/lmc

Technical Information Department
LAWRENCE LIVERMORE LABORATORY
University of California | Livermore, California | 94550